Vol 16 No 3, March 2007
1009-1963/2007/16(03)/0854-08

Chinese Physics

© 2007 Chin. Phys. Soc.
and IOP Publishing Ltd

Dynamic scaling behaviour of late-stage phase separation in $Ni_{75}Al_xV_{25-x}$ alloys*

Li Yong-Sheng(李永胜)†, Chen Zheng(陈 铮), Lu Yan-Li(卢艳丽), and Xu Guo-Dong(徐国栋)

State Key Laboratory of Solidification Processing, Northwestern Polytechnical University, Xi'an 710072, *China*

(Received 8 April 2006; revised manuscript received 20 September 2006)

The dynamic scaling behaviour of late-stage phase separation and coarsening mechanisms of $L1_2$ and $D0_{22}$ in $Ni_{75}Al_xV_{25-x}$ ($3 \le x \le 10$, at.%) alloys are studied using the microscopic phase-field dynamic model. The microelasticity field is incorporated into the diffusion dynamic model. The results show the morphology and coarsening dynamics being greatly changed by the elastic interactions among different precipitates, the particles aligning along the dominant directions, the average domain size (ADS) of $L1_2$ and $D0_{22}$ deviating from the exponent of temporal power-law, and the growth slowing down due to the increasing of elastic interactions. The dynamic scaling regime of late-stage coarsening of the precipitates is attained. Thus the scaling behaviour of structure function is also applicable for elastic interaction systems. It is also found that the variations of ADS and scaling function depend on the volume fraction of precipitates.

Keywords: phase separation, dynamic scaling, elastic interaction, microscopic phase-field simulation
PACC: 8130M, 6470K, 6150K

1. Introduction

The late-stage phase coarsening dynamics in a phase separating alloy has been studied in both theory and technology for many years.[1−5] For alloy systems where the lattice styles in matrix and precipitates are the same and the origin of the coarsening behaviour is that its interfacial energy tends to reduction, they seem to have some common features in both the morphology and the growth rate of the domains. In such systems, the average domain size (ADS) $< R >$ obeys the power-law $R(t) \sim t^n$ with a characteristic growth exponent of $n = 1/3$, which was first derived by Lifshitz and Slyozov,[6] and Wagner[7] and is usually referred to as the LSW theory. However, this is valid only for the growth of an infinitesimally small volume fraction of precipitates in a dilute fluid matrix. Moreover, the spatial quantity scale, such as the time-dependent structure factor $S(k,t)$ displays the scaling behaviour $S(k,t) = R(t)^d F(kR(t))$, where d is the dimensionality of the system and $F(x)$ is the time-independent scaling function. This indicates that the essential features of the morphology only depend on the volume fraction of precipitates.

In the multiphase alloy systems, the presence of the elastic fields induced by the lattice mismatch of different phases strongly changes the morphology as well as coarsening dynamics,[8,9]so that the universal features of the LSW growth disappear,[10] the system follows other kinetic alternatives during the phase separation. It has been found that anisotropic elastic interactions lead to the formation of very anisotropic, mostly platelike precipitates. The predominant alignment of precipitates in certain crystallographic directions is due to the elastic interactions. Nevertheless, with respect to the growth of domain, their typical size still grows in many cases as $t^{1/3}$.[11−13] However, some resent results report a considerable reduction in the growth rate in the late-stage coarsening.[14−17] For some alloy systems, the domains growth appears to stop after the precipitates have reached a certain critical size. The effects of elastic stress on the coarsening dynamics have not yet been well established. So investigating the dynamic scaling behaviour of two-phase coexistent systems is helpful to understanding the problem of phase separation in the presence of elastic interactions.

In this paper, we investigate the dynamic scaling and coarsening mechanisms of late-stage phase separation of $L1_2$ and $D0_{22}$ in $Ni_{75}Al_xV_{25-x}$ alloy sys-

*Project supported by the National Natural Science Foundation of China (Grant No 50071046) and the National High Technology and Development Program of China (Grant No 2002AA331050), and the Doctorate Foundation of Northwestern Polytechnical University of China (Grant No CX200507).

†E-mail: ysli@mail.nwpu.edu.cn

tems with the microscopic phase-field model. The $Ni_{75}Al_xV_{25-x}$ alloys undergo the phase transformation fcc→$L1_2(Ni_3Al)$ + $D0_{22}(Ni_3V)$ at 1281 K.[18] Pareige and Blavette[19] have simulated the kinetic reaction by using Monte Carlo method. Tanimura *et al*[20] investigated the pattern bifurcation related to the $L1_2$ →$D0_{22}$ structure change and the final equilibrium state experimentally. The precipitates have different structures in matrix, so the elastic interactions are included in the microscopic phase-field model. We assume that the precipitates have the same elastic constants (i.e. elastically homogeneous), and this approach has been extensively used in computer simulation of coherent precipitate morphology and coarsening dynamics.[21−23]

2. Model and numerical methods

2.1. Microscopic phase-field dynamic model

The microscopic phase-field dynamic model was founded by Khachaturyan,[24] which is the Onsager-type diffusion equations. In this model, the atomic configurations and morphologies are described by single-site occupation probability function, $x(r,t)$, which is the probability that a given lattice site r is occupied by an atom at time t. The change rates of these probabilities are linearly proportional to the thermodynamic driving force

$$\frac{\partial x(r,t)}{\partial t} = \sum_{r'} L(r-r')\frac{\delta F}{\delta x(r',t)}, \tag{1}$$

where F is the free energy function of $x(r',t)$, $L(r-r')$ is the symmetry matrix of microscopic kinetics related to the probability of an elementary diffusion jump from sites r to r' per unit time. This model has been used to simulate the ordering and decomposition of binary and ternary alloy systems that do not include the elastic interactions.[25]

In the ternary systems, the occupation probability functions $P_A(r,t)+P_B(r,t)+P_C(r,t)=1$, so there are only two equations independent at each lattice site. In order to describe the nucleation, we add a random thermal noise to the right-hand side of the equation. Thus the microscopic Langevin equations[26] are given by

$$\begin{aligned}\frac{\mathrm{d}P_A(r,t)}{\mathrm{d}t} &= \frac{1}{k_BT}\sum_{r'}\Big(L_{AA}(r-r')\frac{\partial F}{\partial P_A}(r',t) \\ &\quad + L_{AB}(r-r')\frac{\partial F}{\partial P_B}(r',t)\Big) + \xi(r,t), \\ \frac{\mathrm{d}P_B(r,t)}{\mathrm{d}t} &= \frac{1}{k_BT}\sum_{r'}\Big(L_{BA}(r-r')\frac{\partial F}{\partial P_A(r',t)} \\ &\quad + L_{BB}(r-r')\frac{\partial F}{\partial P_B}(r',t)\Big) + \xi(r,t), \end{aligned} \tag{2}$$

where $L_{\alpha\beta}(r-r')$ is a constant related to the exchange probabilities of a pair of atoms, α and β, at lattice site r and r' per unit time, α, β = A, B or C. k_B is the Boltzmann constant. $\xi(r,t)$ is assumed to be Gaussian-distributed with an average value of zero, which is uncorrelated with space and time, and it obeys the so-called fluctuation dissipation theory. F is the total free energy of the system,

$$\begin{aligned} F = -\frac{1}{2}\sum_r\sum_{r'}&(V_{AB}(r-r')P_A(r)P_B(r') \\ &+ V_{BC}(r-r')P_B(r)P_C(r') \\ &+ V_{AC}(r-r')P_A(r)P_C(r')) \\ &+ k_BT\sum_r(P_A(r)\ln(P_A(r)) \\ &+ P_B(r)\ln(P_B(r)) + P_C(r)\ln(P_C(r)))\,, \end{aligned} \tag{3}$$

where $V_{\alpha\beta}(r-r') = V_{\alpha\beta}(r-r')_{at} + V_{\alpha\beta}(r-r')_{el}$ is the interaction energy between α and β at the lattice sites r and r', including short-range chemical interaction $V_{\alpha\beta}(r-r')_{at}$ and long-range strain-induced interaction $V_{\alpha\beta}(r-r')_{el}$.

2.2. Microelasticity field

In the linear elasticity theory of multi-phase coherent solid developed for the homogeneous modulus case, the strain energy generated by an arbitrary concentrations or structure-heterogeneity can be presented as a functional of the concentration or the long-range order parameter field. Therefore, it can be easily incorporated into the field dynamic equations. If we assume that the strain is predominantly caused by the concentration heterogeneity, which is the case for the Ni-based superalloys, and if the Vergard's law (the lattice parameter is linearly dependent on composition) is applicable, the configuration-dependent part of the strain energy can be expressed in an extremely simple form of pairwise interaction.[17] The long-range strain-induced interaction associated with an arbitrary atomic distribution $p(r)$ is given by

$$E_{el} = \frac{1}{2}\sum_{rr'} V_{\alpha\beta}(r-r')_{el}P_\alpha(r)P_\beta(r'). \tag{4}$$

As the decomposition process is determined by the development of a packet of concentration waves with wave vectors close to zero, the long-wave approximation for the Fourier transform of $V_{\alpha\beta}(r-r')_{\rm el}$ can be used as follows:

$$V_{\alpha\beta}(k)_{\rm el} \approx M(n) = M_{\rm el}\varepsilon_0^2(\boldsymbol{n}_x^2\boldsymbol{n}_y^2 - \langle \boldsymbol{n}_x^2\boldsymbol{n}_y^2\rangle), \quad (5)$$

$\boldsymbol{n} = \boldsymbol{k}/k$ is the unit vector in the reciprocal space, and ($\boldsymbol{n}_x$, $\boldsymbol{n}_y$) are the Cartesian coordinates of a unit vector n, $\varepsilon_0 = da(c)/(a_0 dc)$ is the concentration coefficient of crystal lattice parameter, $a(c)$ is the lattice parameter of a solid solution with concentration c, a_0 is the lattice parameter of pure solvent, and $\langle \boldsymbol{n}_x^2\boldsymbol{n}_y^2\rangle$ is the average of $\boldsymbol{n}_x^2\boldsymbol{n}_y^2$.

$$M_{\rm el} = -\frac{4(C_{11}+2C_{12})^2}{C_{11}(C_{11}+C_{12}+2C_{44})}\zeta, \quad (6)$$

where $\zeta = C_{11} - C_{12} - 2C_{44}$ characterizes the elastic anisotropy of the system, $C_{i,j}$ is the elastic constants of Ni-based solid solution, which are $C_{11} = 209.2$ GP, $C_{12} = 149.3$ GP, $C_{44} = 96.2$ GP at 1000 K.[27]

The elastic strain energy is given by a dimensionless parameter $\xi = M_{\rm el}\varepsilon_0^2/\Delta f$, where $\xi = 1200$ is an input datum, Δf is the local chemical free energy. The parameter ε_0 can be estimated from the lattice misfit and the concentration diversity, for example, for the alloy with $x = 5.3$, the inputting $\varepsilon_0 = 0.039$.

2.3. Scaling behaviour analysis

During the late-stage coarsening, the spatial patterns at two different times are related by a global change of the length scale, proportional to the average domains size $R(t)$. The late-stage evolution of the system can be described in terms of scaling with $R(t)$. The time-dependent structure function can measure the strength of spatial correlations in the order parameter with wave k, at time t, which is defined as

$$S(k,t) = \frac{1}{N}\Big\langle \sum_r \sum_{r'} [C(r+r',t) \times C(r',t) - C_0^2]\mathrm{e}^{-\mathrm{i}kr} \Big\rangle, \quad (7)$$

where both sums run over the lattice of liner size L and $N = L^2$ is the total number of points in the lattice, $C(r)$ is the local composition, and C_0 is the overall composition. The circularly averaged structure function is

$$S(k,t) = \frac{\sum\limits_{k-\Delta k/2<|k|<k+\Delta k/2} S(k,t)}{\sum\limits_{k-\Delta k/2<|k|<k+\Delta k/2} 1}, \quad (8)$$

where $k = |k|$. The normalized structure function is defined as

$$s(k,t) = \frac{S(k,t)}{\sum_k S(k,t)} = \frac{S(k,t)}{N[\langle C^2(r)\rangle - C_0^2]}. \quad (9)$$

The late-stage coarsening process can be described in terms of scaling with a time-dependent length. This characteristic length represents a measure of the typical domain size and increases with time. If a microstructure exhibits scaling, it means that the structure remains invariant with time and is only scaled or magnified in length as it evolves. There are several ways to characterize the typical length scale $R(t)$, such as $k_{\rm m}(t)$, the location of the maximum of $s(k,t)$, and $k_1(t)$, the inverse of first moment of $s(k,t)$. It is difficult to measure $k_{\rm m}(t)$ because of the discretization, so we use $k_1(t)$ as an equivalent measurement. It is expressed as

$$k_1(t) = \frac{\sum ks(k,t)}{\sum s(k,t)}. \quad (10)$$

With this definition, the scaling function based on the structure function is

$$G(kR,t) = G(k/k_1,t) = k_1^d(t)s(k,t), \quad (11)$$

where d is dimensionality of the system and G is the time-dependent scaling function. If the structure function is scaled, then we expect to have

$$G(k/k_1,t) = g(k/k_1). \quad (12)$$

3. Results and discussion

3.1. Coarsening law and mechanism

Figure 1 shows the atomic-scale configuration variation of $L1_2$ and $D0_{22}$ in a $Ni_{75}Al_{5.3}V_{19.7}$ alloy system at late-stage coarsening. The simulated pictures are depicted with different grey levels: if the occupation probability of vanadium is 1.0, then that site is white, so $D0_{22}$ phases are white; if the occupation probability of aluminium is 1.0, then that site is black, so the $L1_2$ phases are black; the colour of matrix is grey. The simulation is performed with 256×256 mesh points，and a periodical boundary condition is imposed along both dimensions.

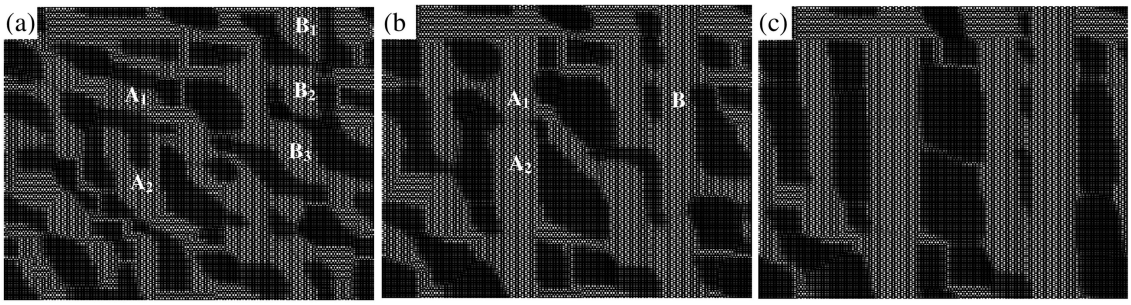


Fig.1. Microstructure evolution of alloy with $x = 5.3$ at 1020 K. (a) $t^* = 20$; (b) $t^* = 80$; (c) $t^* = 190$. Particles A_1, A_2, B_1, B_2 and B_3 in (a) are $D0_{22}$ before coalescence, particle B in (b) is coalesced by B_1, B_2 and B_3 at [100] directions.

It can be seen that the particles align along a certain preferential direction as the coarsening progresses. As the three $< 001 >$ directions are crystallographically equivalent for the $L1_2$ structure, the preferential alignment direction of $L1_2$ particles is the $< 001 >$ direction. But the $D0_{22}$ has three different variants, so in the 2-D projection picture, the two directions [100] and [001] exhibit different preferential alignments. The particles A_1, A_2, B_1, B_2, and B_3 shown in Fig.1(a) are $D0_{22}$ particles. As the coarsening progresses, the $D0_{22}$ particles align along the dominant [100] direction, the B_1, B_2, and B_3 coalesce into a big particle B, and A_1 and A_2 form the interphase boundaries along this direction as shown in Fig.1(b). The average aspect ratio of $D0_{22}$ is plotted in Fig.2, and it can be seen that the aspect ratio increases with time going. Finally, the two-phase particles result in a plates shape and they are parallel to each other, for this state has a lower energy than when they are perpendicular to each other. Akaiwa and Voorhees[28] and Thornton *et al*[29] also observed this phenomenon. The appearance of a dominant variant can also be understood on the basis of elastic energy calculation of plates. Khachaturyan *et al*[30] and Doi and Miyazaki *et al*[31] showed that the plates aligned parallel to each other in an elastic energy minimizing configuration.

To quantify the growth of the precipitates, many studies focus on the numerical values of the growth exponents. The value of the growth exponent is mostly the signature of the mechanism for driving the phase separation process, e.g. $n = 1/3$ for LSW growth. However, the late-stage coarsening slows down due to the presence of elastic interactions. Moreover, some systems such as the Ti–Mo, coarsening appears to stop after the precipitates have reached a certain critical size.[32] So we concentrate on general features and trends of the ADS $R(t)$. It should be pointed out that the domain area S is a more valid representation of domain size as opposed to the radius R. The domain size is approximated by $R = \sqrt{S}$. The ADS $R(t)$ at a given time is obtained by averaging over all the domains in the system.

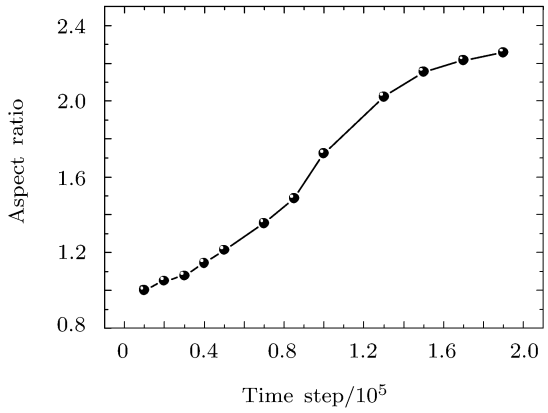


Fig.2. Average aspect ratio of $D0_{22}$ as a function of time.

Figure 3 plots the cube of ADS as a function of time for $L1_2$and $D0_{22}$ in alloy with $x = 5.3$ at 1020 K and 1120 K. It can be seen from Fig.3(a) that the coarsening process slows down dramatically after 1×10^5 time steps, and the cube of ADS vs time at late-stage coarsening shows the asymptotic linear behaviour. The ADS value of $L1_2$ is a little greater than that of $D0_{22}$ at 1020 K. However, the asymptotic linear behaviour is indistinct at 1120 K, as shown in Fig.3(b), and the ADS also exhibits the accelerated growth at early-time and slowing down at late-stage. The magnitude of $D0_{22}$ ADS is greater than that of $L1_2$ after 4×10^5 time steps, and almost equal finally. As the alloy lies in the middle transition regions, the

relative magnitudes of ADS of two phases change with temperature. The results indicate that the increasing elastic interactions in the late-stage slow down the coarsening processes, and the ADSs of two phases are not required to obey the growth law.

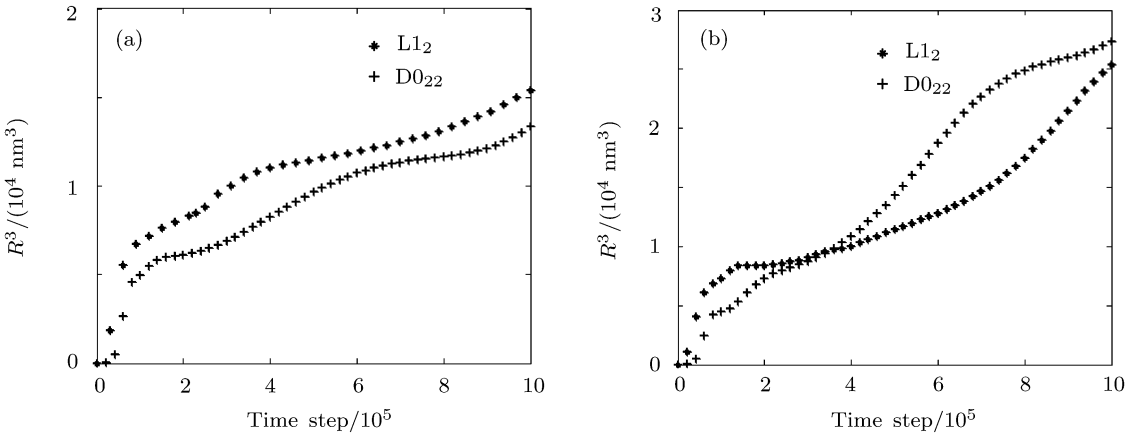


Fig.3. Cube of average domain size of precipitates as a function of time for alloy with $x = 5.3$ at $T = 1020$ K (a) and $T = 1120$ K (b).

The ADS variation in low concentration regions ($x = 4.2$) is plotted in Fig.4. Figure 4(a) shows the cube of ADS vs time of $L1_2$ at different temperatures. It can be seen that the ADSs of $L1_2$ are qualitatively similar at different temperatures, and decrease with the temperature falling. The ADS variation also has the early-time and late-stage characteristics. But the ADS of $D0_{22}$ exhibits the different behaviours at the higher temperatures (1230 and 1120 K) as shown in Fig.4(b): the ADS increases rapidly after 2×10^5 time steps, and then effectively freezes over 6×10^5 time steps. This is due to the coalescence of $D0_{22}$ in the [100] direction at the coarsening stage, which forms the bigger particles. For the lower temperatures (1020 K), the ADS also increases rapidly at the late-stage, but less than for higher temperatures, so the ADS is smaller than that for higher temperatures. It can be seen from Fig.4 that the final magnitude of the ADS of $D0_{22}$ is greater than that of $L1_2$ for each temperature.

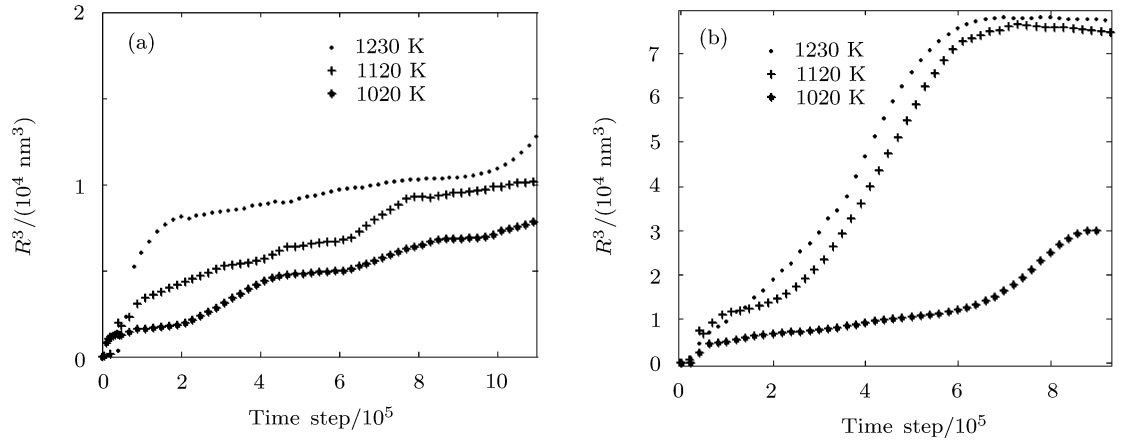


Fig.4. Cube of average domain size of $L1_2$ (a) and $D0_{22}$ (b) as a function of time for alloy with $x = 4.2$ at different temperatures.

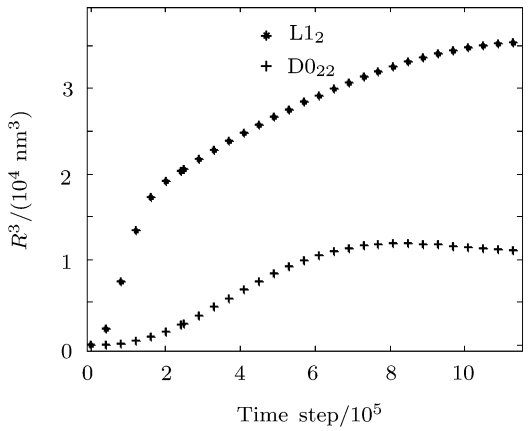


Fig.5. Cube of average domain size of precipitates as a function of time for alloy with $x = 9.2$ at 1120 K.

Figure 5 shows the two phases ADSs for alloy with $x = 9.2$ at 1120 K. It is obvious that the ADS of $L1_2$ is greater than that of $D0_{22}$, and the variation characteristics are similar to those in low and middle concentration regions. So it can be concluded that with the Al concentration increasing the ADS of $L1_2$ increases, whereas the ADS of $D0_{22}$ decreases. The coarsening behaviour of the precipitates in the $Ni_{75}Al_xV_{25-x}$ alloy disagrees with the classical LSW theory. The coarsening mechanisms of $L1_2$ and $D0_{22}$ incorporated with the elastic field are the combination of neighbouring particles, or the growth in certain dominant directions, such as the [100] direction of $D0_{22}$.

3.2. Dynamic scaling

Figure 6 shows the 'law' data for $s(k,t)$ at seven different times during the evolution. The most noticeable features from the structure function are the increase in the maximum value of the structure function and the shift towards lower k values of the position of maximum, with time going. Experimentally, the structure function is a spherical average of scattered intensity as a function of the scattering vector k. According to the small-angle scattering (SAS) technique, the physical interpretation of an increase in maximum is associated with the microstructure evolution towards equilibrium, while a decrease in position of maximum is related to an increase in the characteristic length scale of the particles. It should be pointed that the characteristics of structure functions of $L1_2$ and $D0_{22}$ are similar, despite their different precipitation orders, which shows that the late-stage coarsening of the two phases takes place simultaneously. The difference in structure function between $L1_2$ and $D0_{22}$ is that the maximum value of $L1_2$ is greater than that of $D0_{22}$ for the alloy with $x = 5.3$.

Chakrabarti *et al*[33] have proved that the dynamic scaling is satisfied with different volume fractions at late-stage phase separation and changes with the volume fraction. Tokuyama *et al*[34] have predicted that the shape of scaling function strongly depends on the volume fraction in three dimensions for the small volume fractions. Fratzl *et al*[35] also have pointed out that the scaling function is dependent on volume fraction but independent of temperature. For the $Ni_{75}Al_xV_{25-x}$ alloys, the precipitation order of two-phase changes sequentially with the concentration: the $L1_2$ precipitates first in low concentration regions and $D0_{22}$ precipitates first in high concentration regions.

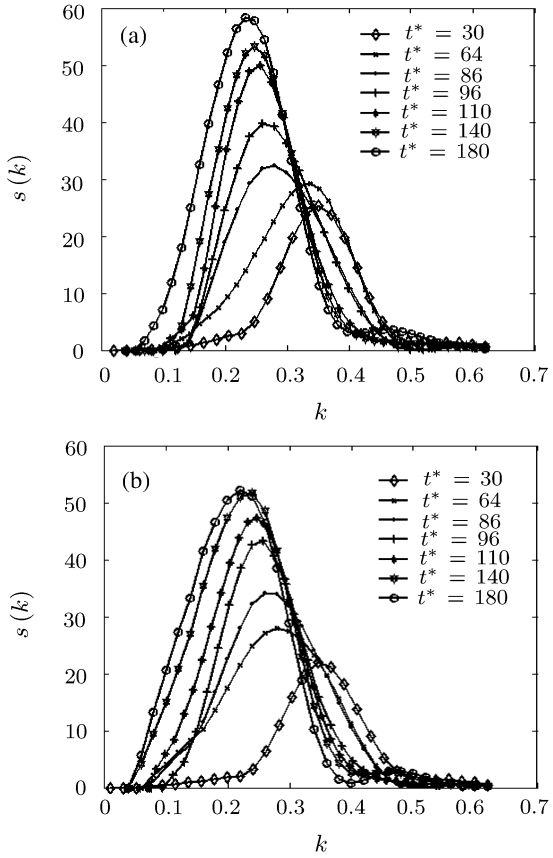


Fig.6. Normalized structure function vs k as a function of time for alloy with $x = 5.3$ for $L1_2$ (a) and $D0_{22}$ (b).

Now we make a comparison among the qualitative features of the scaling functions for different concentration regions. Figure 7 shows the scaling functions of $L1_2$ and $D0_{22}$ obtained from the normalized structure functions. It can be seen that after $t^* = 120$, the scaling data for six different times satisfy the same dis-

tribution law, indicating that the scaling regime has been attained for both of the two phases. The shapes of the scaling functions for $L1_2$ and $D0_{22}$ are very similar, and the difference is that the peak value of $L1_2$is greater than that of $D0_{22}$, which is similar to the behaviour of structure function.

Figure 8(a) shows the scaling functions of $L1_2$ and $D0_{22}$ for alloy with $x = 8.3$ at 1230 K. It can be seen that the peak value of $D0_{22}$ is greater than that of $L1_2$. But for alloy with $x = 4.2$ at 1120 K, the peak value of $L1_2$ is greater than that of $D0_{22}$ as shown in Fig.8(b), which is similar to that of alloy with $x = 5.3$ at 1020 K. So it can be concluded that the relative peak height of the scaling function changes from a value of $D0_{22}$ higher than that of $L1_2$ to a value lower than that of $L1_2$ as the $L1_2$ volume fraction decreases. Despite the different peak values of the scaling function, the shapes are very similar for the two phases in the different concentration regions.

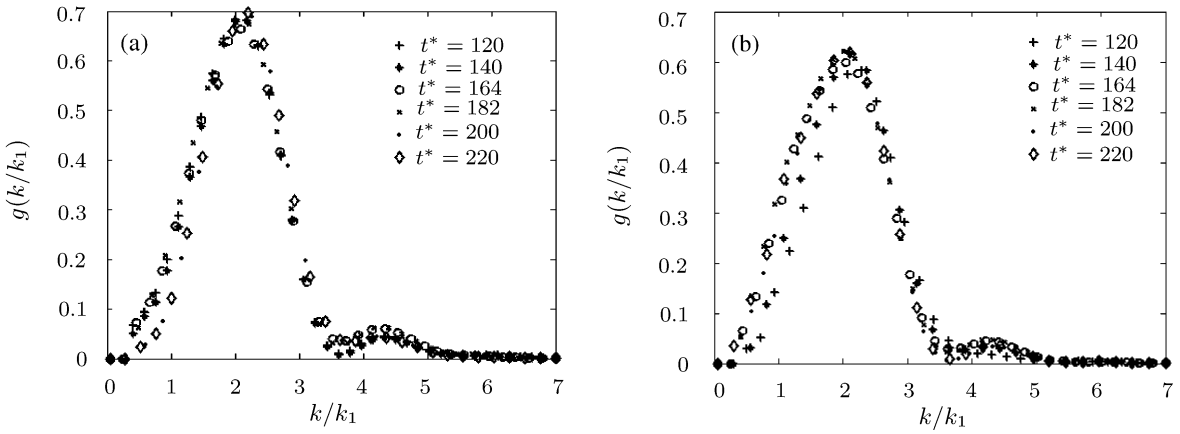


Fig.7. Scaling function as a function of k/k_1 from six different times for alloy with $x = 5.3$ for $L1_2$ (a) and $D0_{22}$ (b).

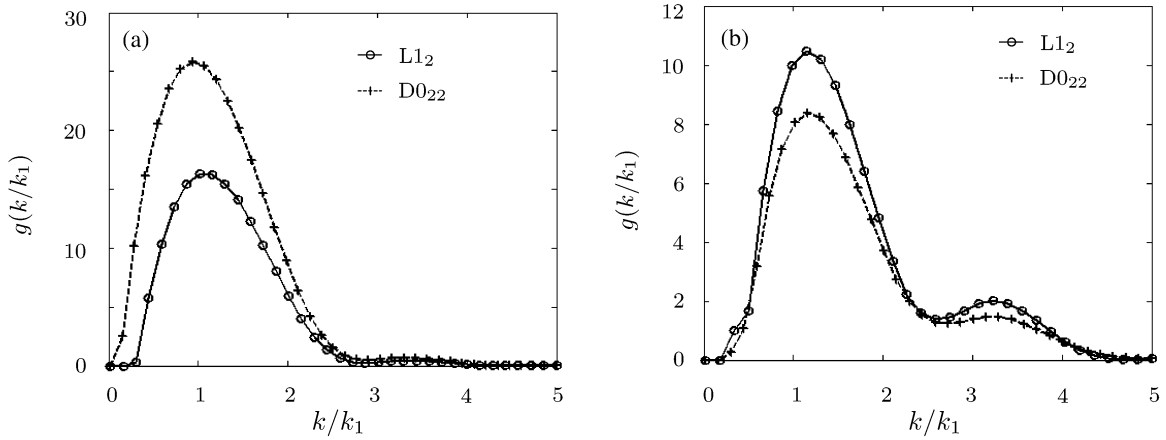


Fig.8. Scaling functions as a function of k/k_1 for $L1_2$ and $D0_{22}$ for the alloy with $x = 8.3$ at $T = 1230$ K (a) and the alloy with $x = 4.2$, $T = 1120$ K (b).

4. Conclusion

In conclusion, we have investigated the dynamic scaling behaviour and coarsening mechanisms of $L1_2$ and $D0_{22}$ in $Ni_{75}Al_xV_{25-x}$ alloy systems using the microscopic phase-field model incorporated with the elastic field. Due to the lattice mismatch between different particles, the process of phase separation radi-

cally changes due to the presence of long-range elastic field. Both of the two phases exhibit the preferential alignment directions at the late-stage phase separation. The coarsening process has the characteristic of growth accelerated at early-time and slowing down at late-stage, which results from the adding of elastic interactions. However, the quick increase of the ADS of $D0_{22}$ during growth is induced by the particles coalescence along the dominant direction. So the scaling rule of LSW theory is inapplicable for the growth of $L1_2$ and $D0_{22}$. In addition, The scaling regime of late-stage coarsening is attained for $L1_2$ and $D0_{22}$ in the $Ni_{75}Al_xV_{25-x}$ alloy. It is interesting that the relative magnitude of ADS of $L1_2$ is greater than that of $D0_{22}$ in high concentration regions, and less than that of $D0_{22}$ in low concentration regions, but the relative peak height of the scaling function of $L1_2$ is less than that of $D0_{22}$ in high concentration regions, and that is reversed in low concentration regions. The results imply that the scaling behaviour of structure function is also applicable for the elastic interaction systems.

The quantitative features of the late-stage coarsening process are described in the present simulations. However, the limit system size and the difference in elastic constant between the matrix and the particles may make the statistics insufficient in accuracy. Nevertheless, it may be possible to develop an exact form of growth law and scaled structure function of two-phase systems involving the elastic interactions in much large systems and their quantitative descriptions.

References

[1] Paris O, Fahrmann M and Fratzl P 1995 *Phys. Rev. Lett.* **75** 3458

[2] Chai Z G, Meng F L, Zou Q and Wang Y M 2002 *Chin. Phys.* **11** 191

[3] Muralidharan G and Chen H 2000 *Sci. Technol. Adv. Mater.* **1** 51

[4] Du Z W, Zhou T T, Zhao H, Feng L P, Dong B Z and Chen C Q 2004 *Acta Phys. Sin.* **53** 3601 (in Chinese)

[5] Shao Y Z, Lai J K L, Shek C H, Lin G M and Lan T 2004 *Chin. Phys.* **13** 243

[6] Lifshitz I M and Slyozov V V 1961 *J. Phys. Chem. Solids.* **19** 35

[7] Wangner C 1961 *Z. Elektrochem.* **65** 581

[8] Rogers T M, Elder K R and Desai R C 1998 *Phys. Rev.* B **37** 9638

[9] Wang K G, Glicksman M E and Rajan K 2005 *Comp. Mater. Sci.* **34** 235

[10] Calderon H A, Kostorz G, Qu Y Y, Dorantes H J, Cruz J J and Cabanas-Moreno J G 1997 *Mater. Sci. Eng.* A **238** 13

[11] Laberge C A, Fratzl P and Lebowitz J L 1995 *Phys. Rev. Lett.* **75** 4448

[12] Gorentsveig V I, Fratzl P and Lebowitz J L 1997 *Phys. Rev.* B **55** 2912

[13] Sagui C, Orlikowski D, Somoza A M and Roland C 1998 *Phys. Rev.* E **58** R4092

[14] Nishimori H and Onuki A 1990 *Phys. Rev.* B **42** 980

[15] Wen Y H, Wang Y and Chen L Q 2002 *Acta Mater.* **50** 13

[16] Ges A, Fornaro O and Palacio H 1997 *J. Mater. Sci.* **32** 3687

[17] Wang Y, Chen L Q and Khachaturyan A G 1992 *Phys. Rev.* B **46** 11194

[18] Takeyama M and Kikuchi M 1998 *Intermetallics* **6** 573

[19] Pareige C and Blavette D 2001 *Scr. Mater.* **44** 243

[20] Tanimura M, Kikuchi M and Koyama Y 2002 *J. Phys.: Condens. Matter* **14** 7053

[21] Thornton K, Akaiwa N and Voorhees P W 2001 *Phys. Rev. Lett.* **86** 1259

[22] Semenovskaya S and Khachaturyan A G 1998 *J. Appl. Phys.* **83** 5125

[23] Li X F 2005 *Comp. Mater. Sci.* **34** 70

[24] Khachaturyan A G 1983 *Theory of Structural Transformation in Solids* (New York: Wiley) p129

[25] Poduri R and Chen L Q 1998 *Acta Mater.* **46** 1719

[26] Chen L Q 1994 *Acta Metall. Mater.* **42** 3503

[27] Prikhodko S V, Carnes J D, Isaak D G and Ardell A J 1998 *Scr. Mater.* **38** 67

[28] Akaiwa N and Voorhees P W 2000 *Mat. Sci. Eng.* A **285** 8

[29] Thornton K, Akaiwa N and Voorhees P W 2001 *Phys. Rev. Lett.* **86** 1259

[30] Khachaturyan A G, Semenovskaya S V and Morris Jr J W 1988 *Acta Metall.* **36** 1563

[31] Doi M, Miyazaki T and Wakatsuki T 1985 *Mat. Sci. Eng.* **74** 139

[32] Langmayr F, Fratzl P, Vogl G and Miekeley W 1994 *Phys. Rev.* B **49** 11759

[33] Chakrabarti A, Toral R and Gunton J D 1993 *Phys. Rev.* E **47** 3025

[34] Tokuyama M, Enomoto Y and Kawasaki K 1987 *Phys.* A **143** 183

[35] Fratzl P, Lebowitz J L, Penrose O and Amar J 1991 *Phys. Rev.* B **44** 4794